Polymer 236 (2021) 124298

Contents lists available at ScienceDirect

Polymer

journal homepage: www.elsevier.com/locate/polymer

Easy-way production of highly transparent nanocellular polymers films

J. Martín-de León [a,*], M. Jiménez [a], J.L. Pura [d], V. Bernardo [b], M.A. Rodriguez-Pérez [a,c]

[a] Cellular Materials Laboratory (CellMat), Condensed Matter Physics Department, University of Valladolid, Valladolid, 47011, Spain
[b] CellMat Technologies S.L. Paseo de Belen 9A, 47011, Valladolid, Spain
[c] BioEcoUVA Research Institute on Bioeconomy, University of Valladolid, Spain
[d] Gds Optronlab, Condensed Matter Physics Department, Universidad de Valladolid, 47011, Spain

ARTICLE INFO

Keywords:
Transparent nanocellular PMMA
Gas dissolution foaming
Transparent poymer films

ABSTRACT

The key parameters and production route for the easy production of highly transparent nanocellular films based on polymethylmethacrylate (PMMA) with thickness below 1 mm are herein described.

The use of the gas dissolution foaming process (CO_2 as physical blowing agent) with saturation pressures of 40 and 50 MPa, a saturation temperature of 0 °C and a saturation time of 2.5 h together with an adequate approach to foam the samples leads to the production of directly transparent nanocellular PMMA with relative densities in the range of 0.47–0.80 and cell sizes in the internal part of the film ranging 23–29 nm.

The produced materials present maximum transparency of 61% for a thickness of 0.5 mm without any post-processing, a value comparable to the one previously obtained in the literature for nanocellular PMMA produced using a long-lasting process that included additional time-consuming post-processing of the samples.

The produced cellular materials have been in-deep characterized, and the influence of several key parameters such as the solid skin thickness, transition region, and cellular structure on the final optical transmittance has been studied.

1. Introduction

Nanocellular polymers have been proved to be promising cellular materials. Scientific papers claiming their reduced thermal conductivity through the gas phase due to Knudsen effect [1–3] or experiments demonstrating their improved mechanical properties can be found in the literature for nanocellular materials based on different polymeric matrices [4–7].

On the other hand, transparent nanocellular polymers were an optimistic hypothesis until the year 2017 were the first transparent nanocellular polymers based on polymethylmethacrylate (PMMA) were reported [8]. These novel materials have a very unusual combination of properties (low thermal conductivity, excellent mechanical properties, low density, hydrophobicity, and transparency), and due to this, they could find applications in several industries. For instance, they could be used as glass substitutes in windows in the building and transport industries. One of the building sector's challenges is to find ways to ensure proper thermal insulation due to the current demanding energetic regulations [9], and it is known that an important part of the energy is lost through the windows [10].

In addition, these materials have been claimed to be useful for protection films in electronic devices (mobile phones or tablets) or for their use in transparent disposable face masks, films for greenhouses, among others.

Besides the material's transparency, all of the proposed applications have an additional request in common to turn this material into an industrial reality; the possibility of a cost-effective and simple production method.

In our previous papers focused on the production of transparent nanocellular PMMA we used the gas dissolution foaming process (CO_2 as physical blowing agent) and very low saturation temperatures (−32 °C) [8,11]. These low saturation temperatures resulted in an extremely long-lasting production process, where the whole saturation process implies several days. Thus, 2 days and 15 days were used to produce nanocellular polymers with 2 and 4 mm in thickness, respectively. In addition, the produced materials needed demanding post-processing (cutting with a precision cutting machine to a lower thickness) after the gas dissolution foaming process to obtain a thin film of transparent material. One important aspect of this post-processing approach is that the solid skin and transition region, typical for materials produced using the gas dissolution foaming process, were removed from the characterized samples, so the samples' transmittance was only affected by the

* Corresponding author.
E-mail address: jmadeleon@fmc.uva.es (J. Martín-de León).

https://doi.org/10.1016/j.polymer.2021.124298
Received 11 April 2021; Received in revised form 22 September 2021; Accepted 20 October 2021
Available online 28 October 2021

relative density and nanocellular structure.

Thus, the idea is the production of thin films presenting transmittances withouth any post-procesing needed. Some papers in the literature claimed the production of very thin films (smaller than 130 nm) from different copolymers and cell sizes as small as 20 nm. However no transparency is claimed for those materials and the thickness is so small to be used in the previously commented applications [12–14].

This work presents alternative production process parameters that allow achieving cellular structures able to provide a significant degree of transparency with a reduced processing time. Increasing the saturation pressure up to 40 and 50 MPa allows increasing the saturation temperature up to 0 °C, without modifying the nanocellular polymer's characteristics, with the consequent reduction in the cycle time. Moreover, an alternative post-saturation foaming approach is proposed, leading to the possibility of producing flat and transparent nanocellular PMMA with thickness in the range of 0.7–1 mm without any post-processing required. These materials are characterized by the presence of a solid skin, a transition region, and an inner nanocellular structure. All parameters defining this complex structure influence the optical properties. An in-deep analysis of the factors influencing the final transparency of the samples has been carried out.

2. Materials and methods

2.1. Materials

PMMA has been kindly supplied by ALTUGLAS® International (Colombes, France). The selected grade for this work was V825T. Provided in the form of pellets, it presents a density of 1.19 g/cm^3 (measured at 23 °C and 50% HR), a molecular weight of M_n = 43 kg/mol, and M_w = 83 kg/mol (measured through gel permeation chromatography) and a glass transition temperature (T_g) of 114 °C (measured through differential scanning calorimetry).

The melt flow index (MFI) of this polymer has been measured to be 1.92 g/10 min (160 °C/10 Kg), and it presents a zero-shear viscosity of 7095 Pa s measured through shear rheology [15].

This grade of PMMA was selected because it presents the adequate viscosity for the production of cells below 50 nm as it was previously reported in the literature [11,15].

Medical grade CO_2 (99.9% purity) has been used for the gas dissolution experiments.

2.2. Samples production

2.2.1. Precursors production

Solid samples 15 x 15 × 0.5 mm^3 were produced through compression molding with a cold/hot plate press from Remtex (Barcelona, Spain) from the as-received pellets.

Pellets were first dried overnight at 70 °C under vacuum. Afterward, they were compression-molded using a circular mold with 175 mm in diameter and 0.5 mm in thickness. This process consists of three steps. The material is first heated at 250 °C for 9 min under no pressure. A pressure of 8 MPa is later applied in the second step by maintaining the temperature at 250 °C for an additional minute. Finally, the material is cooled down to room temperature in the cold plates under the same pressure of 8 MPa.

The obtained 0.5 mm in thickness solid sheets are machined to the desired dimensions (15 × 15 mm^2) for the foaming tests.

2.2.2. Cellular materials production

To produce the cellular materials, the gas dissolution foaming technique was used [16]. Gas dissolution foaming consists of three steps, saturation, depressurization, and foaming. During saturation, the gas diffuses inside the polymer under certain conditions of saturation pressure (P_{sat}) and temperature (T_{sat}). When the polymer is completely saturated after the so call saturation time (t_{sat}), the gas is released at a fast depressurization velocity (v_{des}) in the depressurization step. This fast reduction of pressure creates a thermodynamic instability that triggers nucleation. The presence of the gas inside the polymer entails a reduction of the glass transition temperature up to the effective glass transition temperature ($T_{g_{eff}}$). Finally, in the foaming step, the polymer is introduced in a foaming set-up at a foaming temperature (T_f) higher than the $T_{g_{eff}}$ during the foaming time (t_f), allowing the nucleation sites to create cells. If T_{sat} is higher than the effective glass transition temperature, the polymer can expand during depressurization. In this case, the process is called one-step foaming.

During the time between depressurization and foaming (desorption time (t_{des})) a part of the gas is diffusing out of the sample (Fig. 1a), creating a gas profile. The maximum amount of gas (C_0) in the center of the sample results in the homogeneous nanocellular region (NR). This amount of gas decreases through sample's thickness [17]. Since gas concentration is critical for the foaming step, this gas profile implies the formation of both a solid skin (SS) and a gradient from higher to smaller cells named as transition region (TR) (Fig. 1b).

The area presenting the maximum solubility results in the cellular structure corresponding to the used saturation conditions. As gas concentration is reduced, a smaller number of larger cells appear, this region of larger cells can be named transition region. In the outer part, where the concentration is below a certain value (C_{min})the foaming temperature do not trespass the $T_{g_{eff}}$ resulting in a region with no cellular structure, giving as a result solid skin. Both regions, transition region, and solid skin, are considered in this work due to their influence on the optical properties.

Gas dissolution foaming experiments have been carried out in the set-up shown in Fig. 2. Samples were saturated in a pressure vessel model High Pressure Chemical Reactor, provided by Supercritical Fluid Technologies (5). This pressure vessel allows working up to 69 MPa of pressure and temperatures between −40° and 200°. The system comprises a pressure pump (2) (model SFT-10 from Supercritical Fluid Technologies), providing the system with the desired pressure. The temperature is controlled through a chiller (7) (model AD15R-40-A11B 15L supplied by Polyscience), connected to a thermal jacket (6). After saturation, samples were foamed in a hot-plate stirrer (Fig. 2b). A polymeric sheet (9) is placed above the sample during foaming to prevent bending.

The investigated parameters for the samples' production have been 40 and 50 MPa for the saturation pressure by keeping the saturation temperature at 0°. Those conditions have been kept constant during a saturation time of 2.5 h to ensure the samples' complete saturation.

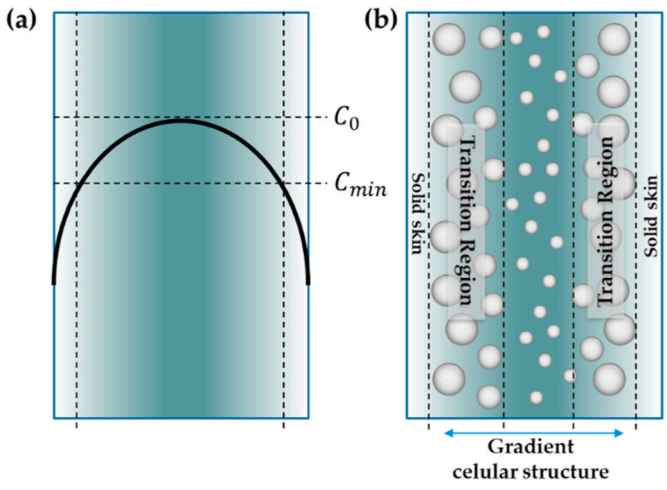

Fig. 1. a) Gas concentration profile in the sample thickness. **b)** Solid skin and gradient cellular structure due to the gas concentration profile in the sample thickness.

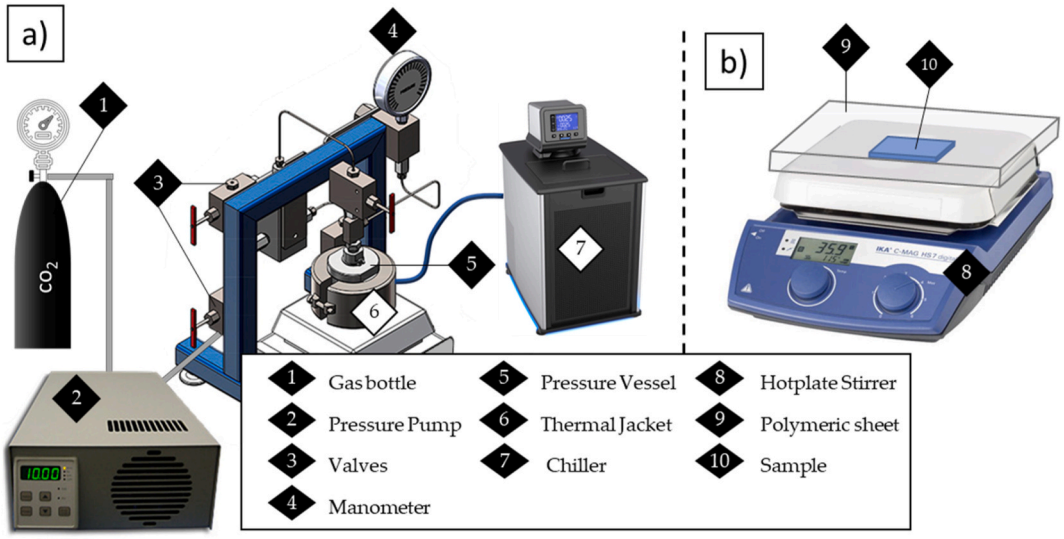

Fig. 2. **a)** Scheme of the pressure system set-up. **b)** Scheme of the foaming set-up.

After saturation, the pressure was released at 100 MPa/s. Finally, samples were foamed after a desorption time of 90 s, under foaming temperatures of 25, 40, and 60 °C with a constant foaming time of 1 min.

2.3. Characterization techniques

2.3.1. Solubility and diffusivity

Solubility was determined as the percentage of weight increment of the sample after gas sorption. A Mettler-Toledo balance was used to register the mass lost vs. time. The mass was later represented as a function of the square root of time divided by sample thickness, and this curve was used to extrapolate to zero time the mass of the samples after saturation. The extrapolated value is considered the sample's mass when it is fully saturated; the material's solubility is calculated using this value [18].

Besides, the same curve was used to determine the desorption diffusivity using the slope method [17].

2.3.2. Density

Density of the solid PMMA (ρ_s) was measured through gas pycnometry (Mod. AccuPyc II 1340, Micromeritics, Norcross, GA, USA), while cellular materials' density (ρ_f) was determined by considering the water displacement method, based on Archimedes' principle with a density determination kit of an AT261 Mettler-Toledo balance.

The density of the cellular materials samples (ρ_f)keeping the samples as obtained after the foaming process, it means considering the solid skin and the transition region, has been measured. Besides, density of the inner nanocellular region has been measured by removing the solid skin and transition region by polishing (200 μm of each side of the samples were removed).

Relative density (ρ_r) is calculated as the ratio between both measured densities: ($\rho_r = \rho_f/\rho_s$).

2.3.3. Scanning electron microscopy

The visualization of the obtained cellular structure was carried out in an ESEM Scanning Electron Microscope (QUANTA 200 FEG, Hillsboro, OR, USA).

Samples were prepared for the visualization. Firstly they were fractured under liquid nitrogen, ensuring to keep the cellular structure intact. Then they were gold coated with a sputter coater (model SDC 005, Balzers Union, Balzers, Liechtenstein). The obtained micrographs were analyzed through a software-based on ImageJ/FIJI [19]. This way, the parameters defining the cellular structure of the inner part of the samples were determined. The cell size (φ) is given by the average of the size of more than 200 cells, the standard deviation divided by the cell size (SD/φ) is also provided. Cell nucleation density (N_0) was determined through Kumar's method [16], the relative density of the inner nanocellular region were used to determine this value.

Additionally, in this paper, the solid skin and the transition region thicknesses (see section 2.2.2) were determined (Fig. 3). Both regions are easily differentiated in the ESEM micrographs, as it is shown in Fig. 3, solid skin is clearly delimited by a line that divides the region without cellular structure of the region with cellular structure. At the same time, the transition region can be identified by a clear color change. At least six measurements have been taken along the samples to determine the thickness of both regions (top and bottom); the presented value is the mean value of these measurements. Regions in both sizes of the sample were measured, proving that structure is symmetrical. Cellular structure of the transition region has been also characterized.

2.3.4. Transmittance measurements

The transmittance is defined as the ratio between the intensity of

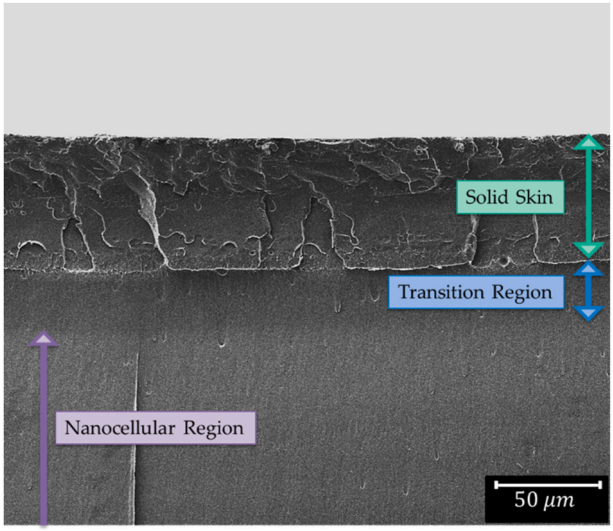

Fig. 3. Scanning electron micrograph showing the solid skin and the transition region of a sample saturated at 40 MPa and 0 °C of saturation pressure and temperature and foamed at 60 °C during 1 min.

light through the sample (I) and the incident intensity (I_0) ($T = I/I_0$). The transmittance values provided are normalized by the solid transmittance of PMMA (this value is around 0.95 for the used thickness and wavelength).

To compare transmittance values for samples presenting different thicknesses, the following relationship has been used:

$$T = T_0^{\frac{l}{l_0}} \quad (1)$$

Where T_0 is the measured transmittance for the thickness of the sample, l_0, and T is the transmittance for a different thickness l. This relationship is based on Beer-Lambert law, proved to be valid for these polymeric materials [20]. With the aim of comparison, the transmittance for a thickness (l) of 0.5 mm has been calculated for all the produced samples.

The used device comprises a green laser of 553 nm of wavelength acting as a light source and a detector based on a photodiode inside an integrating sphere with a 12.5 mm window (PRW0505, Gigahertz-Optik) connected to a photometer (X94, Gigahertz- Optik). To measure the transmitted intensity, samples are placed in contact with the integrating sphere window so as to collect all the transmitted light. The laser-detector distance was fixed as 30 mm, being at this distance the diameter of the laser beam in the sample surface of 2 mm.

2.3.5. Modeling

Light transmission through nanocellular PMMA has been modeled, allowing to evaluate the light interaction with the cellular structures obtained. The commercial software COMSOL Multiphysics has been used for this purpose. The used algorithm is described in a previously published paper [11].

3. Results

3.1. Solubility and diffusivity

Solubility and diffusivity as a function of saturation conditions are shown in Table 1. Thus 40 MPa of saturation pressure combined with a saturation temperature of 0 °C leads to a solubility of 42 wt% of gas while increasing P_{sat} up to 50 MPa raises solubility to 46 wt%.

According to the literature a solubility higher than 40% is necessary to obtain cell sizes below 50 nm with this grade of PMMA. As it can be seen the used parameters in this work leads to solubilities above this value. In addition the amount of gas obtained at 50 MPa and 0 °C is similar to the maximum solubility value of 48 wt % reported in the literature for PMMA [8]. This solubility was achieved by using 20 MPa and −32 °C as saturation conditions. Such low saturation temperature implied saturation times of 7 h for samples 0.5 mm in thickness.

It can be concluded that an equivalent amount of gas is achievable by an increase in the saturation pressure from 20 to 50 MPa while increasing the saturation temperature from −32 °C to 0 °C. To saturate a 0.5 mm thickness sample, this temperature change reduces the saturation time from 7 to 2.5 h, which means a reduction of 64% in the saturation time.

The increase in the saturation temperature also implies an increment in almost one order of magnitude regarding the desorption diffusivity. Thus, samples saturated at 40 MPa and 0 °C present a desorption diffusivity of $1.46{\cdot}10^{-6}$ cm^3/s, value that rises up to $1.76{\cdot}10^{-6}$ cm^3/s for a saturation pressure of 50 MPa, while the highest value presented for a T_{sat} of −32 °C and 20 MPa was $1.93 \cdot 10^{-7}$ cm^3/s [8]. This value should be carefully considered. By using the current saturation conditions desorption time should be minimized so as to preserve the necessary amount of gas to produce cell sizes below 50 nm.

Table 1
Solubility and diffusivity for the used saturation conditions.

Saturation conditions	Solubility (% CO_2)	Diffusivity (cm^2/s)
40 MPa 0 °C	42	$1.46{\cdot}10^{-6}$
50 MPa 0 °C	46	$1.76{\cdot}10^{-6}$

Considering that CO_2 for both sets of saturation conditions is in liquid state and presents comparable density and viscosity [21], this increase in diffusivity could be attributed to the PMMA matrix. The presence of CO_2 inside the polymeric matrix reduces the effective glass transition as previously commented. In the case of PMMA, the literature shows a reduction up to −12.5 °C when the solubility is around 40 %CO_2 [22]. According to Chow's model, this reduction tends to an equilibrium; thus the $T_{g_{eff}}$ slightly decreases for higher solubilities [22]. In the present case, as solubility is similar for both saturation temperatures, the reduction of the T_g should also be similar. Then, when working at −32 °C, the matrix is below its effective Tg, so the polymeric chains are more rigid than for 0 °C. This effect is enhanced by solid skin presence; in the outer part of the sample, the amount of gas is small, and therefore the $T_{g_{eff}}$ in this region is almost the original one. Consequently, the outer part supposes a harder barrier for the gas at −32 °C than when working at 0 °C.

3.2. Transparent nanocellular films

As described in section 2.2.2, this work introduces a different approach to foam the samples. The foaming step in gas dissolution foaming is usually performed in a thermal bath. However, in this work, samples were foamed on a hot plate. A 0.2 mm aluminum sheet previously preheated at the same temperature as the hot plate is placed above the sample so as to obtain thermal homogeneity. This allows the samples under study to grow completely plane-parallel, as shown in Fig. 4.a.

When working with thin samples, 0.5 mm in thickness, it is not easy to obtain flat foamed materials. Samples saturated at the same conditions were foamed in a thermal bath with the aim of comparison. As shown in Fig. 4.a the PMMA sample completely bends by foaming through this method. Using the hot plate for the foaming step allows eliminating this inconvenience to produce thin flat samples.

The as-obtained sample foamed in the hot plate, with a final thickness of 0.65 mm, present in addition, high transparency without any post-processing (Fig. 4.b.). The showed transparency can be compared with a sample produced at 31 MPa and 24 °C presenting cell sizes around 225 nm [23], that with the same thickness, is completely opaque.

3.3. Relative density and cellular structure

Relative density of the obtained samples, as well as the cellular structure, have been determined (Table 2). As explained in the experimental section, density has been measured with and without polishing. Without polishing the value includes the solid skin and the transition region's influence (Fig. 5a), while after polishing only the density of the nanocellular region is measured (Fig. 5b). The relative density for both used pressures decreases when the foaming temperature is increased. Values near 0.8 are obtained when foaming at 25 °C; these values decrease to 0.59 and to 0.47 for 40 and 50 MPa, respectively for the density of the whole sample.

Although the general tendency remains the same, all values are reduced when considering only the nanocellular region. Thus, maximum values of 0.66 for 40 MPa and 0.52 for 50 MPa are measured for samples foamed at 25 °C while minimum values of 0.44 for 40 MPa and 0.36 for 50 MPa are achieved for 60 °C of T_f. This reduction is attributed to the solid skin removal, this solid skin is thicker for 25 °C as it is later explained and therefore the reduction of density is stronger for this temperature.

When analyzing the cellular structure of the inner nanocellular region, the evolution with the saturation pressure and foaming temperature follows the tendency observed in previous works (Fig. 6). A higher pressure results in smaller cell sizes and higher cell nucleation densities. While increasing the foaming temperature results in only minor

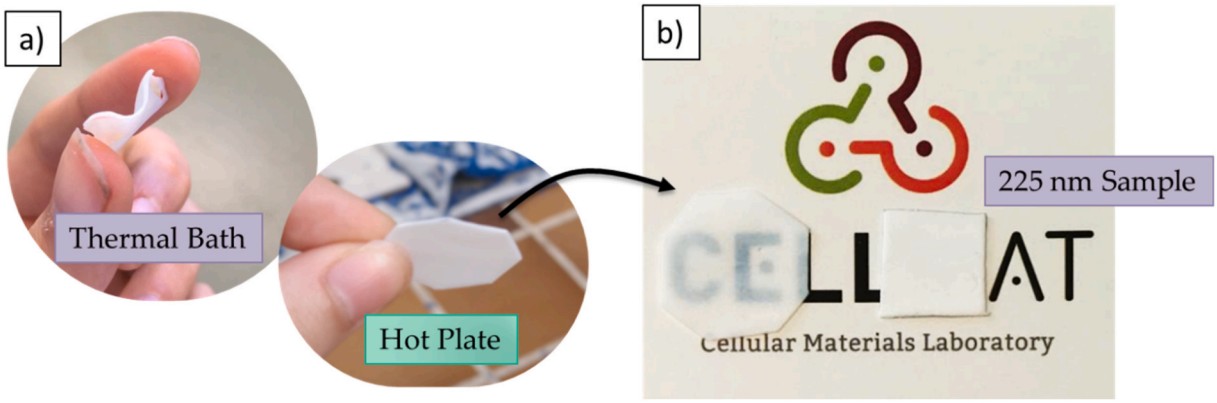

Fig. 4. **a)** Example of two samples saturated at 50 MPa and 0 °C of saturation conditions and foamed at 40 °C in a thermal bath (left sample) and a hot plate (right sample) during 1 min. **b)** Example of the transparency of a sample saturated at 50 MPa and 0 °C and foamed at 40 °C with a thickness of 0.65 mm as produced (left sample) in comparison with a sample produced at 31 MPa and 24 °C and foamed at 40 °C, presenting a cell size of 225 nm.

Table 2
Foaming temperature, relative density of the whole sample, relative density of the inner part, cell nucleation density, cell size, SD/Φ, thickness of the solid skin, and thickness of the transition region for the produced samples.

Saturation conditions	T_f (°C)	ρ_r Whole sample	ρ_r Inner cellular structure	N_0 (nuclei/cm^3)	Φ (nm)	SD/φ	t_{SS} (μm)	t_{TR} (μm)
40 MPa 0 °C	25	0.75	0.66	$7.8{\cdot}10^{15}$	27	0.31	138	8
	40	0.68	0.62	$9.9{\cdot}10^{15}$	27	0.32	100	19
	60	0.59	0.44	$1.5{\cdot}10^{16}$	29	0.33	50	28
50 MPa 0 °C	25	0.79	0.52	$1.3{\cdot}10^{16}$	23	0.26	133	21
	40	0.55	0.43	$2.9{\cdot}10^{16}$	25	0.34	77	32
	60	0.47	0.36	$3.9{\cdot}10^{16}$	25	0.33	21	56

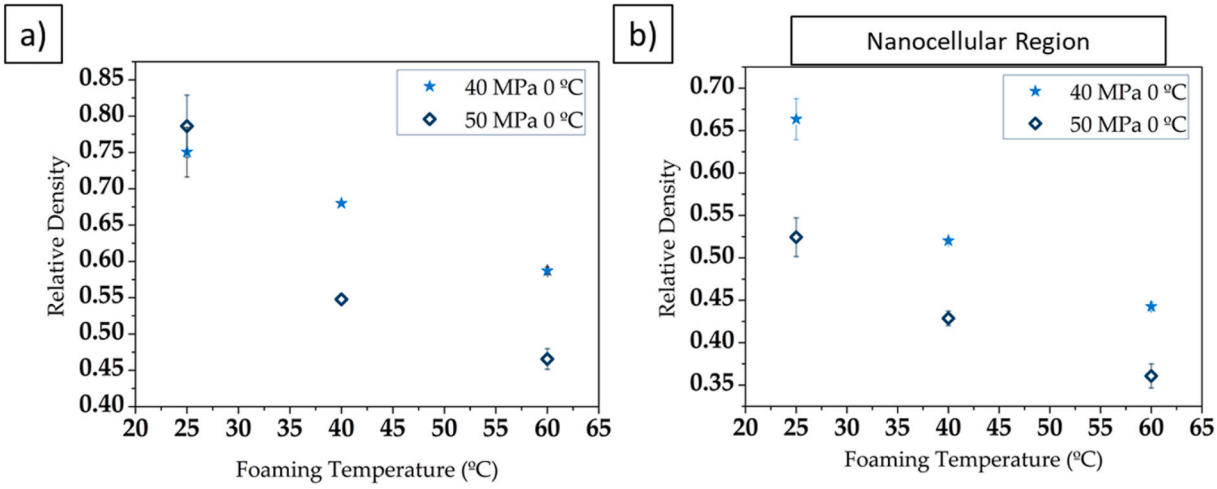

Fig. 5. **a)** Relative density as a function of foaming temperature for 40 MPa, 0 °C and 50 MPa, 0 °C of saturation conditions. **b)** Relative density of the nanocellular region as a function of foaming temperature for 40 MPa, 0 °C and 50 MPa, 0 °C of saturation conditions.

modifications in the cell size, with values around 27 nm for 40 MPa and around 24 nm for 50 MPa. However, the modification of foaming temperature allows increasing the cell nucleation density. At 25 °C, both pressures lead to similar cell nucleation densities of $7.8{\cdot}10^{15}$ nuclei/cm^3 at 40 MPa and $1.3{\cdot}10^{16}$ nuclei/cm^3 at 50 MPa, while raising the foaming temperature up to 60 °C maximizes this value for both pressures, up to $1.5{\cdot}10^{16}$ nuclei/cm^3 for 40 MPa, and more than double at 50 MPa with a maximum of $3.9{\cdot}10^{16}$ nuclei/cm^3.

The higher cell nucleation density leads to reducing the sample's density, explaining the observed difference between densities at 40 and 50 MPa.

The parameter SD/φ shows values near 0.3 for all the analyzed samples, indicating homogeneous cellular structures with narrow cell size distributions.

The minimum cell size obtained at 50 MPa and 0 °C in this work is comparable to the one obtained at 10 MPa and −32 °C in the literature (24 nm) [11]. It can be concluded that similar nanocellular structures can be obtained with a reduction of 64% in the saturation time.

As previously discussed, the solid skin and the transition region are vital for transparent materials production. Fig. 7 shows the proportion (in thickness) of these two regions for the studied process parameters. Although the solid skin thickness is slightly higher for 40 MPa than for 50 MPa, it sharply decreases for both pressures when increasing the foaming temperature. At 25 °C of foaming temperature, it comprises 20 (40 MPa) and 24% (50 MPa) of the total thickness while this value decreases to 7.6% (40 MPa) and 3% (50 MPa) at 60 °C.

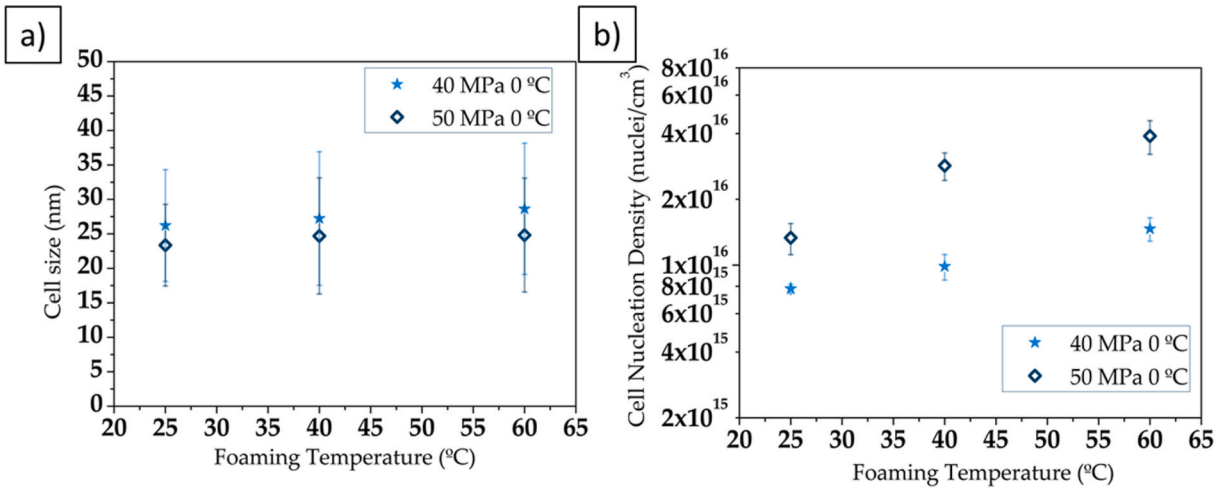

Fig. 6. a) Cell size as a function of foaming temperature for 40 MPa, 0 °C, and 50 MPa, 0 °C of saturation conditions. **b)** Cell nucleation density as a function of foaming temperature for 40 MPa, 0 °C and 50 MPa, 0 °C of saturation conditions.

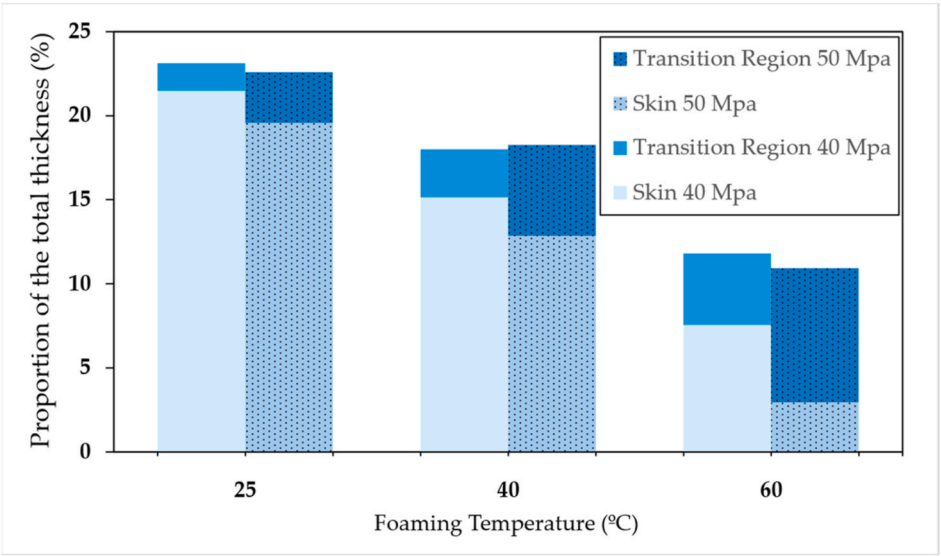

Fig. 7. a) Solid skin and transition region as a function of foaming temperature for 40 and 50 MPa and 0 °C of saturation conditions.

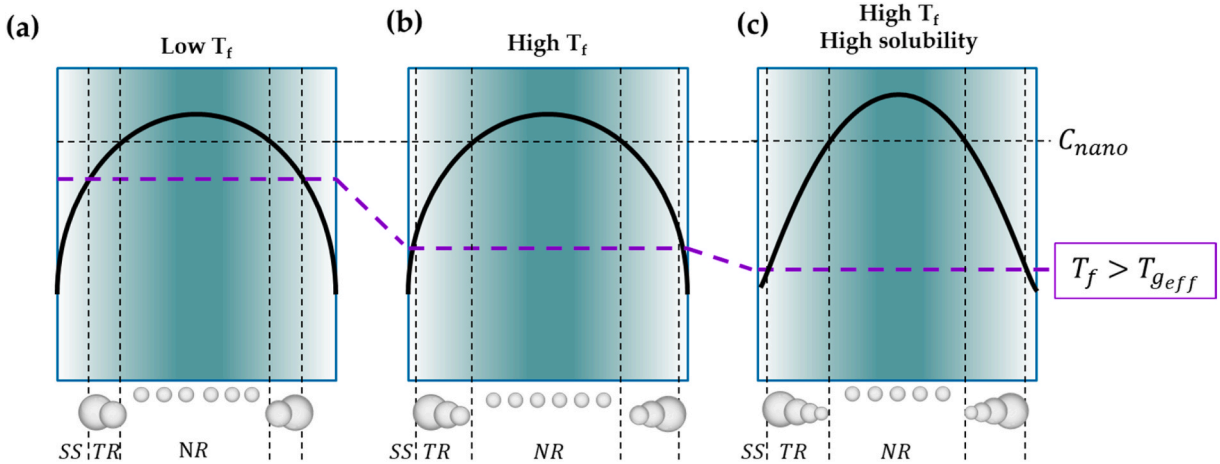

Fig. 8. a) Solid skin and transition region as a function of foaming temperature for 40 and 50 MPa and 0 °C of saturation conditions.

On the contrary, the transition region thickness is higher for 50 MPa. Also, it increases with the foaming temperature presenting values of 1.6% (40 MPa) and 3% (50 MPa) for 25 °C, and 4.3 (40 MPa) and 8% (50 MPa) for 60 °C.

This can be explained through the gas profile inside the sample (Fig. 8). The profile of the $T_{g_{eff}}$ would be similar to that one of the gas. On the one hand, cellular structure only appears as far as the T_f is higher than the $T_{g_{eff}}$ (above dashed line in Fig. 8). On the other hand, the homogeneous nanocellular region appears above a critical solubility (C_{nano}). Below this gas concentration, and as far as the foaming temperature is higher than $T_{g_{eff}}$, bigger cells are created, generating the transition region.

Working with the same pressure means having the same gas profile inside the sample (Fig. 8.a and **b.**), the $T_{g_{eff}}$ evolution is also equal for both cases. So, for a lower foaming temperature is harder to trespass the effective glass transition. Meaning that the region of the sample above the dashed line is smaller. According with the Figure this leads to thicker solid skin and a thinner transition region in comparison with a higher foaming temperature. When increasing the pressure (Fig. 8c), solubility is higher, this implies a higher diffusivity and a smaller $T_{g_{eff}}$, so the difference between T_f and $T_{g_{eff}}$ decreases. This leads to thinner solid skin and a thicker transition region for higher solubilities.

3.3.1. Transmittance measurements

Transmittance has been measured for the samples obtained after foaming, i.e., considering the transition region and solid skin. Then the transmittance for a thickness of 0.5 mm was calculated for all the materials as explained in the experimental section.

Fig. 9.a shows the transmittance values for all the samples. Those materials produced at 50 MPa lead to higher transmittances than the ones produced at 40 MPa. Besides, an increase in the foaming temperature implies a reduction in the transmittance. While at 40 MPa, the range of transmittances varies from 44% to 25%, at 50 MPa, this range goes from 61% to 47%.

Summarizing, the higher transmittance is obtained when working at 50 MPa and 0 °C of saturation pressure, with a foaming temperature of 25 °C. These values have been compared with the reported data in the previous literature (Fig. 9.b.), showing that the maximum value obtained in this paper is comparable to the one previously reported.

It is, therefore, possible to produce semi-transparent plane sheets of nanocellular materials with 0.5 mm in thickness and transparency as high as 61% in a fast gas dissolution foaming experiment, with no post-processing. As mentioned, a reduction in the production time of 64% was achieved, and the cutting process required in previous reports have been completely removed.

3.3.2. Factors affecting transmittance

The measured samples' transmittance values are affected mainly by four factors: the solid skin, the transition region, the cellular structure characteristics of the inner nanocellular structure and the relative density.

The solid skin's effect on transparency was studied using FEM modeling using an approach previously explained [20]. A nanocellular material with 24 nm of cell size, a relative density of 0.5, and 1.5 μm in thickness was modeled, with and without the presence of solid skin. As shown in Fig. 10, the solid skin introduces light couplings that reduce the transmittance value from 0.99 without solid skin to 0.89 with solid skin.

As the solid skin is completely transparent, its thickness does not affect the whole sample transparency; only its presence does. That means, the presence of the solid skin reduces the transmittance due to light couplings, in comparison with a sample without solid skin. On the other hand, when comparing samples with solid skin, the solid skin's transmittance is the transmittance of the solid that is higher than that of the cellular structure, so when increasing the solid skin proportion, the transmittance will increase.

In order to analyze the effect of the transition region in the transmittance, the cellular structure of this transition region was studied. Fig. 11 shows the inner nanocellular structure and the transition region's cellular structure for a sample produced at 40 MPa and 0 °C foamed at 25 °C. The cell size in the showed transition region is 57 nm.

When talking about transparency in nanocellular polymers, the key factor is to reduce the cell below a tenth of the used wavelength. That means that for visible light, where the medium wavelength of the spectrum is 530 nm, it is necessary to have cells smaller than 50 nm so as to observe some transparency in the material [20,24]. This threshold marks the transition between Mie and Rayleigh scattering. Above 50 nm, the Mie scattering leads to a high amount of scattered light that leads to opaque samples. Below this value, the regime changes, and the amount of scattered light becomes smaller, leading to higher transmittances.

Considering that for the smaller foaming temperature, the cell size in the transition region is already above 50 nm, it can be considered that Mie scattering will govern the transmittance in the TR transition region being the transmittance small and similar independently on the cell size.

Thus, so as to evaluate the effect of the TR in the total transmittance of the sample its thickness is the key parameter (Table 2). Its proportion compared to the thickness of the material presenting cellular structure (total thickness without solid skin thickness) has been calculated, and

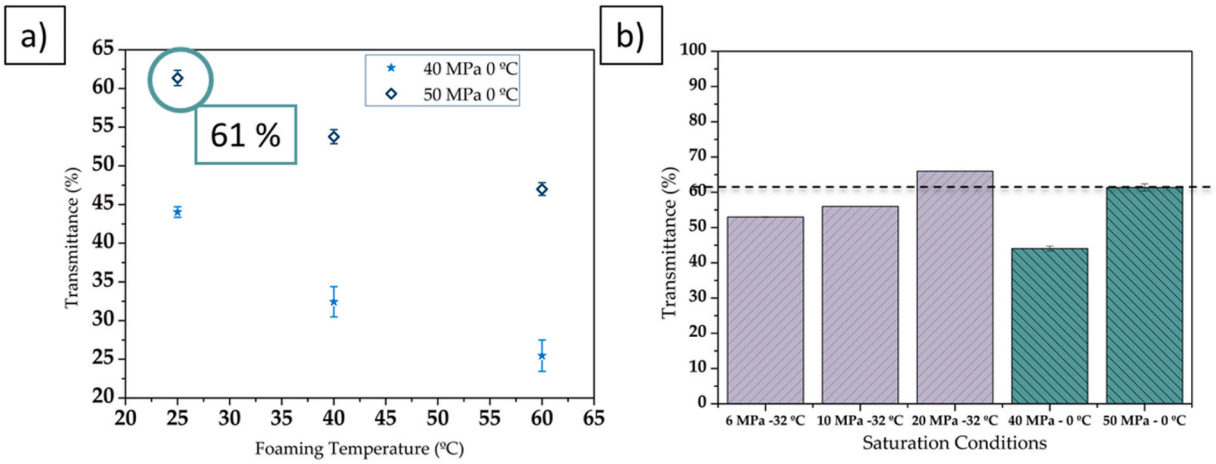

Fig. 9. a) Transmittance as a function of foaming temperature for 40 MPa, 0 °C and 50 MPa, 0 °C of saturation conditions for 0.5 mm samples. **b)** Higher transmittance obtained in this work at 40 and 50 MPa and 0 °C compared to the literature (higher values obtained at 6–20 MPa and −32 °C). Dashed line marking the maximum transmittance in this work in comparison with the previous one.

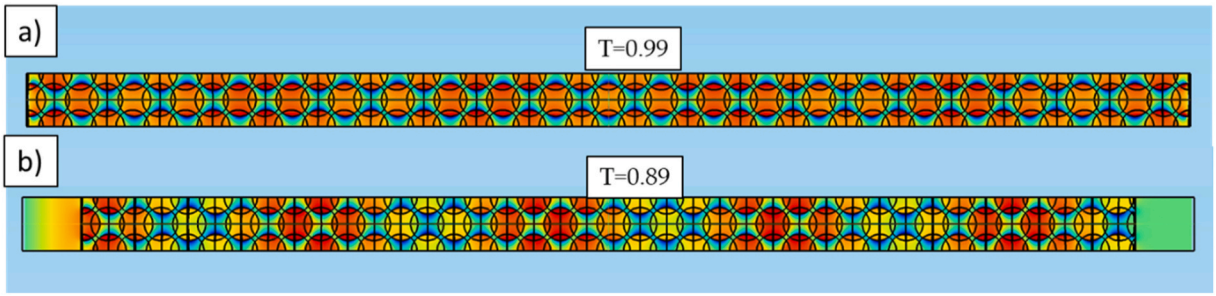

Fig. 10. a) Spatial distribution of electrical field modulus for 24 nm of cell size sample and 1.5 μm in thickness without solid skin. **b)** Spatial distribution of electrical field modulus for 24 nm of cell size sample and 1.5 μm in thickness with solid skin.

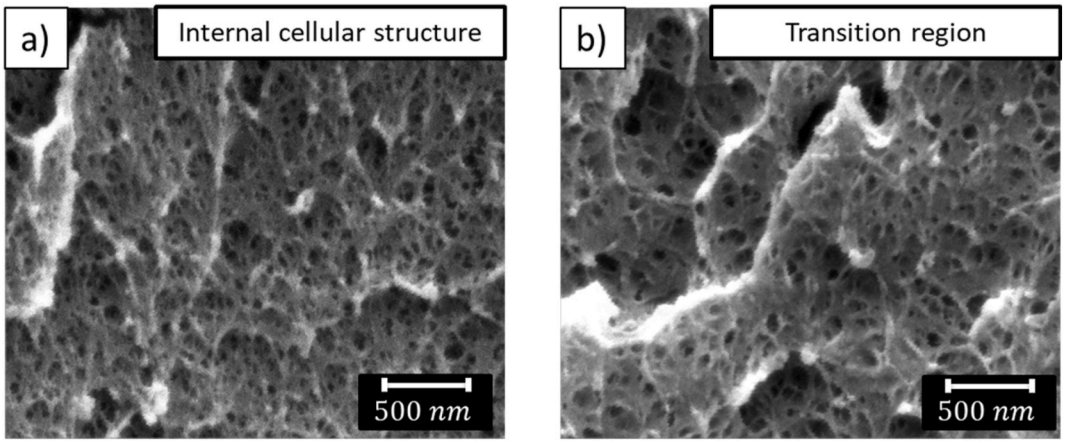

Fig. 11. a) Inner cellular structure of a sample produced at 40 MPa and 0 °C and foamed at 25 °C during 1 min.

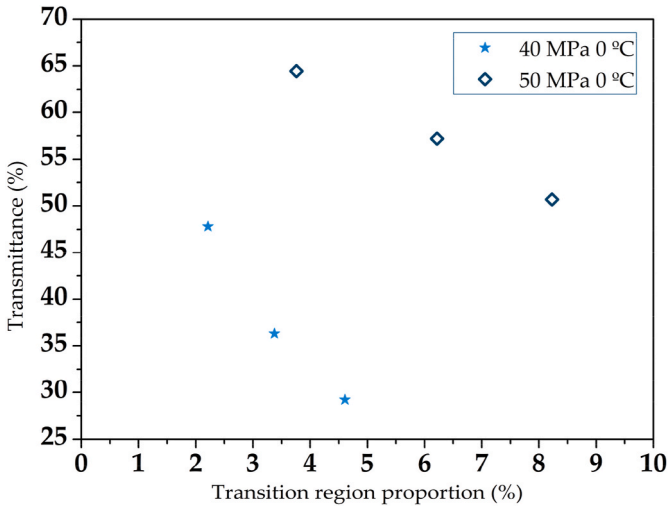

Fig. 12. Transmittance as a function of the transition region proportion for both saturation pressures.

the influence of this proportion on the final transmittance has been analyzed in Fig. 12.

An increase in the transition region thickness, triggered by a higher foaming temperature (Fig. 7), reduces the studied materials' final transmittance. Therefore, it can be concluded that a thicker transition region leads to the reduction of the final transmittance of the material, being essential to minimize this region.

The effect of the cellular structure of the homogeneous region was studied by polishing the samples and removing the thickness of the solid skin and the transition region. It has to be considered that this transmittance includes the superficial defects on the sample created when polishing. As shown in Fig. 13.a, this removal implies a clear improvement of the transmittance when the foaming temperature increases. Firstly, the cell size plays an important role, for both used pressures cell size is below 50 nm, however 50 MPa leads to smaller cell sizes and therefore higher transmittances. On the other hand, when increasing the foaming temperature cell nucleation density increases, which implies a reduction of the relative density of the material. This density reduction implies therefore, an increase in the transmittance.

The four commented factors play an important role in the final transmittance of the sample. As it can be concluded from Fig. 13.b., for non-post-processed samples, a lower saturation temperature is beneficial due to a small transition region despite the reduced cell nucleation density in comparison with the one obtained at a higher temperature. On the other hand, when eliminating the influence of solid skin and transition region, the key role is to maximize the cell nucleation density so minimize the density by increasing the foaming temperature while keeping the cell size below 50 nm.

The samples' post-processing introduces some defects in the sample's surfaces. The transmittance values for this material is slightly higher to the higher transmittance values of the samples without post-processing.

4. Conclusions

Flat PMMA nanocellular layers with less than 1 mm in thickness and high transparency have been produced using the gas dissolution foaming process. The approach presented here is a straightforward process with a short cycle time and allows producing transparent nanocellular materials without any post-processing.

The material used has been PMMA, saturation parameters have been 40 and 50 MPa of saturation pressures and 0 °C of saturation

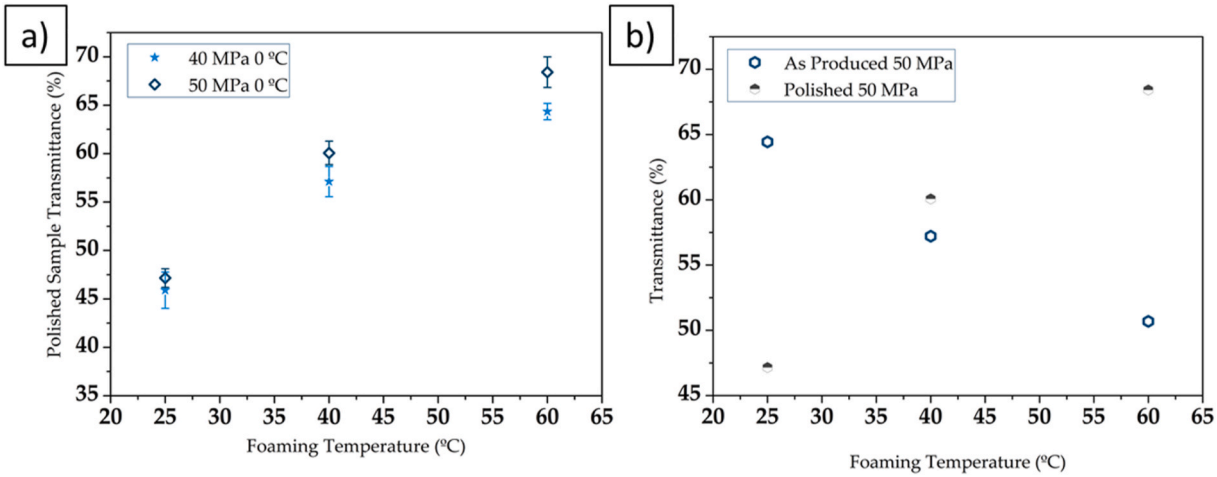

Fig. 13. a) Transmittance of the polished samples as a function of the foaming temperature for both saturation pressures. **b)** Transmittance as a function of foaming temperature for samples at 50 MPa, as produced, and after polishing.

temperature. Foaming temperatures ranging from 25 to 60 °C have been tested. The obtained materials and their transparency have been compared with those produced in a previous work at 6–20 MPa and −32 °C.

Nanocellular PMMA with cell sizes around 24 nm and $1.33 \cdot 10^{16}$ nuclei/cm^3 have been produced through 50 MPa of saturation pressure and foaming in a hot-plate at 25 °C. This sample presents the maximum transmittance of all the produced materials, 61%, for a thickness of 0.5 mm. This value is comparable to the higher one reported in the literature (64%), but this last material was produced with a much longer cycle, and an intense post-processing was needed.

The relationship between the process parameters, the obtained materials structure, and the transmittance has also been studied. It has been proved that for non-processed materials, a thin transition region without a solid skin and the minimization of the cell size and the relative density are the key factors to maximize the transmittance of nanocellular polymers.

CRediT authorship contribution statement

J. Martín-de León: Conceptualization, Methodology, Validation, Formal analysis, Investigation, Writing – original draft, Visualization, Supervision. **M. Jiménez:** Formal analysis, Investigation, Visualization. **J.L. Pura:** Software. **V. Bernardo:** Conceptualization, Methodology, Writing – review & editing. **M.A. Rodriguez-Pérez:** Conceptualization, Methodology, Validation, Writing – review & editing, Supervision, Project administration, Funding acquisition.

Declaration of competing interest

The authors declare that they have no known competing financial interests or personal relationships that could have appeared to influence the work reported in this paper.

Acknowledgments

Financial assistance from the Junta of Castile and Leon (VA202P20) and Spanish Ministry of Science, Innovation, and Universities (RTI2018-098749-B-I00) and the "Ente Público Regional de la Energía de Castilla y León" (EREN) are gratefully acknowledged. Financial support from Spanish Ministry of Science, Innovation, Torres Quevedo Program (PTQ2019-010560: V. Bernardo) is gratefully acknowledged.

References

[1] B. Notario, J. Pinto, E. Solorzano, J.A. De Saja, M. Dumon, M.A. Rodriguez-Perez, Experimental validation of the Knudsen effect in nanocellular polymeric foams, Polym. (United Kingdom). 56 (2015) 57–67, https://doi.org/10.1016/j.polymer.2014.10.006.
[2] C. Forest, P. Chaumont, P. Cassagnau, B. Swoboda, P. Sonntag, Polymer nano-foams for insulating applications prepared from CO2 foaming, Prog. Polym. Sci. 41 (2015) 122–145, https://doi.org/10.1016/j.progpolymsci.2014.07.001.
[3] V. Bernardo, J. Martin-de Leon, J. Pinto, R. Verdejo, M.A. Rodriguez-Perez, Modeling the heat transfer by conduction of nanocellular polymers with bimodal cellular structures, Polymer 160 (2019) 126–137, https://doi.org/10.1016/j.polymer.2018.11.047.
[4] D. Miller, V. Kumar, Microcellular and nanocellular solid-state polyetherimide (PEI) foams using sub-critical carbon dioxide II. Tensile and impact properties, Polymer 52 (2011) 2910–2919, https://doi.org/10.1016/j.polymer.2011.04.049.
[5] R.W.B. Sharudin, M. Ohshima, CO2-induced mechanical reinforcement of polyolefin-based nanocellular foams, Macromol. Mater. Eng. 296 (2011) 1046–1054, https://doi.org/10.1002/mame.201100085.
[6] V. Bernardo, F. Van Loock, J. Martin-de Leon, N.A. Fleck, M.A. Rodriguez-Perez, Mechanical properties of PMMA-Sepiolite nanocellular materials with a bimodal cellular structure, Macromol. Mater. Eng. 304 (2019) 1–12, https://doi.org/10.1002/mame.201900041.
[7] J. Martín-de León, F. Van Loock, V. Bernardo, N.A. Fleck, M.Á. Rodríguez-Pérez, The influence of cell size on the mechanical properties of nanocellular PMMA, Polymer 181 (2019), https://doi.org/10.1016/j.polymer.2019.121805.
[8] J. Martín-de León, V. Bernardo, M.Á. Rodríguez-Pérez, Key production parameters to obtain transparent nanocellular PMMA, Macromol. Mater. Eng. 302 (2017), https://doi.org/10.1002/mame.201700343.
[9] M. Economidou, V. Todeschi, P. Bertoldi, D. D'Agostino, P. Zangheri, L. Castellazzi, Review of 50 years of EU energy efficiency policies for buildings, Energy Build. 225 (2020) 110322, https://doi.org/10.1016/j.enbuild.2020.110322.
[10] B. Nourozi, A. Ploskić, Y. Chen, J. Ning-Wei Chiu, Q. Wang, Heat transfer model for energy-active windows – an evaluation of efficient reuse of waste heat in buildings, Renew. Energy 162 (2020) 2318–2329, https://doi.org/10.1016/j.renene.2020.10.043.
[11] J. Martín-de León, J.L. Pura, V. Bernardo, M.Á. Rodríguez-Pérez, Transparent nanocellular PMMA: characterization and modeling of the optical properties, Polymer 170 (2019) 16–23, https://doi.org/10.1016/j.polymer.2019.03.010.
[12] C. Dutriez, K. Satoh, M. Kamigaito, H. Yokoyama, Nanometer voids prevent crack growth in polymeric materials, Macromolecules 40 (2007) 7433–7436, https://doi.org/10.1021/ma071262p.
[13] L. Li, H. Yokoyama, T. Nemoto, K. Sugiyama, Facile fabrication of nanocellular block copolymer thin films using supercritical carbon dioxide, Adv. Mater. 16 (2004) 1226–1229, https://doi.org/10.1002/adma.200400264.
[14] R. Zhang, C. Dutriez, K. Sugiyama, T. Ishizone, H. Yokoyama, Thermally robust nanocellular thin films of high-Tg semifluorinated block copolymers foamed with supercritical carbon dioxide, Soft Matter 7 (2011) 4032–4038, https://doi.org/10.1039/c0sm00736f.
[15] J.M. León, V. Bernardo, E. Laguna-Gutiérrez, M.Á. Rodríguez-Pérez, Influence of the viscosity of poly(methyl methacrylate) on the cellular structure of nanocellular materials, Polym. Int. 69 (2020) 72–83, https://doi.org/10.1002/pi.5920.
[16] V. Kumar, N.P. Suh, A process for making microcellular thermoplastic parts, Polym. Eng. Sci. 30 (1990) 1323–1329, https://doi.org/10.1002/pen.760302010.
[17] J. Crank, The Mathematics of Diffusion, Oxford University Press, 1975, https://doi.org/10.1016/0306-4549(77)90072-X.

[18] K. Nadella, H. Guo, J. Weller, V. Kumar, Sorption and Desorption of CO 2 in Polycarbonate (PC) and Acrylonitrile Butadiene Styrene (ABS) in the Solid State Microcellular Process, ((n.d.)).
[19] J. Pinto, E. Solorzano, M.a. Rodriguez-Perez, J.a. de Saja, Characterization of the cellular structure based on user-interactive image analysis procedures, J. Cell. Plast. 49 (2013) 555–575, https://doi.org/10.1177/0021955X13503847.
[20] J. Martín-de León, J.L. Pura, V. Bernardo, M.Á. Rodríguez-Pérez, Transparent nanocellular PMMA: characterization and modeling of the optical properties, Polymer 170 (2019) 16–23, https://doi.org/10.1016/j.polymer.2019.03.010.
[21] R. Span, W. Wagner, A new equation of state for carbon dioxide covering the fluid region from the triple-point temperature to 1100 K at pressures up to 800 MPa, J. Phys. Chem. Ref. Data 25 (1996) 1509–1596, https://doi.org/10.1063/1.555991.
[22] H. Guo, V. Kumar, Solid-state poly(methyl methacrylate) (PMMA) nanofoams. Part I: low-temperature CO2 sorption, diffusion, and the depression in PMMA glass transition, Polymer 57 (2015) 157–163, https://doi.org/10.1016/j.polymer.2014.12.029.
[23] J. Martín-de León, V. Bernardo, M.Á. Rodríguez-Pérez, Low density nanocellular polymers based on PMMA produced by gas dissolution foaming: fabrication and cellular structure characterization, Polymers 8 (2016) 265, https://doi.org/10.3390/polym8070265.
[24] D.J. Lockwood, Rayleigh and Mie scattering, in: R. Luo (Ed.), Encycl. Color Sci. Technol., Springer Berlin Heidelberg, Berlin, Heidelberg, 2014, pp. 1–12, https://doi.org/10.1007/978-3-642-27851-8_218-1.